Seismic Event Detection using Bridge Monitoring Data Based on Multi-input Deep Neural Networks

Hao Fang[1], Yao Chen[1*], Zhou Su[1] and Ying He[1]

[1] Yunnan Transportation Science Research Institute Co., Ltd., Kunming, 650011, China
675055573@qq.com

Abstract. Seismic events pose a significant threat to the safety of bridge structures, potentially causing extensive structural damage or collapse. Structural health monitoring (SHM) systems for large-span bridges capture structural response information and generate substantial data but face issues like sensor faults, environmental noise, and data transmission problems that can degrade data quality and hinder accurate seismic response identification. This paper proposes a multi-input deep learning method for seismic event detection, which exploits the correlation between sensors in different directions, especially in the case of sensor failure, to improve detection accuracy. The proposed approach creates an acceleration database, incorporating time-domain, frequency-domain, and probability density curve images as inputs for model training aimed at anomaly classification of sensor data. Then, the multi-input model integrates data from sensors in various orientations, significantly improving the identification rate of seismic events. Meanwhile, a global voting strategy is implemented to optimize the decision-making process during the prediction phase. When applied to actual seismic response data from a cable-stayed bridge, the experimental results confirm the effectiveness of the proposed method in accurately detecting sensor anomalies and identifying seismic events in bridges.

Keywords: Structural health monitoring, Seismic event detection, Large-span bridges, Information fusion, Data anomaly detection.

1 Introduction

Large-span bridges are critical for urban and regional transportation networks, providing essential links across regions and promoting economic growth[1]. These bridges are vulnerable to extreme events, particularly seismic events. The implementation of SHM systems enables real-time monitoring of the bridge's condition, allowing for timely and accurate detection of seismic events that the bridge experiences, thereby facilitating the implementation of emergency measures to mitigate potential losses and risks. The SHM system for large-span bridges generates a large amount of monitoring data, which is instrumental in bridge health evaluation, extreme events identification, service life prediction, and ultimately, ensuring overall

W. Guo et al. (eds.), *Proceedings of the 3rd International Conference on Green Building, Civil Engineering and Smart City (GBCESC 2024)*, Advances in Engineering Research 264,
https://doi.org/10.2991/978-94-6463-728-1_70

safety [2]. Additionally, long-term outdoor deployment exposes most SHM systems to environmental nuisance, leading to sensor faults and introducing anomalies in the monitoring data. Such anomalies caused by sensor faults may compromise the accuracy of structural analyses and potentially lead to incorrect conclusions. Simultaneously, Extreme events like typhoons, ship collisions, and seismic events may lead to abrupt changes in engineering structures, potentially causing structural damage. However, the features of some sensor fault data may be similar to those of the monitoring data during seismic events, making it difficult for the system to identify seismic events accurately. For current research in anomaly detection and extreme event detection, it is common to concentrate on one specific task independently. Meanwhile, existing methods presume the occurrence of an extreme event when the majority of sensors detect such events, overlook the potential influence of sensor orientation, and lack a comprehensive framework for multi-sensor data fusion.

Information fusion technology has recently made significant progress, providing the possibility of fusing multi-sensor information. It entails the efficient transformation of information from varied sources and timeframes into a decision-supportive format [3]. Information fusion algorithms can be categorized based on their specific data processing techniques and underlying theoretical principles, such as probabilistic theory[4], evidence theory[5], decision theory[6], and various machine learning approaches[7]. For example, Liu et al. developed a dam safety early warning system using multi-source information fusion and decision entropy analysis. This system processes large volumes of monitoring data from multiple locations through Bayesian fusion, providing precise real-time diagnostics [8]. Chen et al. utilized rainfall detection, satellite systems, and displacement sensors to detect landslide factors, using generalized evidence theory for data fusion to provide early warnings [9]. Furthermore, Jeong et al. introduced a multimodal approach to identify tunnel construction activities by combining audio and visual data. This method integrates spatial and temporal relationships to more accurately identify multiple machine activities than single-modality models [10].

SHM systems equipped with multi-sensors offer immense potential for autonomous decision-making regarding extreme events. However, current methodologies face limitations. Existing anomaly detection methods often focus solely on extreme events data or anomalous data, neglecting the co-occurrence of the two data types. Furthermore, these methods disregard sensor orientation, hindering the accurate integration of multi-sensor data and compromising the system's decision-making capacity about seismic events. To address these shortcomings, we present a multi-input deep learning approach for seismic event detection within SHM systems. The main content of the article is as follows: (1) The proposed method utilizes real-world, multi-direction sensor data from a long-span bridge, enabling simultaneous identification of seismic events amidst anomalous data patterns. (2) To achieve the decision-making capabilities within SHM systems for seismic events, we design a deep learning approach that explores multi-input feature fusion, and sufficiently validated in experiments to demonstrate the robustness. Simultaneously, a comparative study of different feature channel inputs was conducted.

2 Methodology

The overview of the proposed method is shown in Fig. 1. In the first step, a real-world monitoring dataset consisting of four types of anomaly and seismic response data was collected from a large-span cable-stayed bridge. Then, the raw time series data are split into sections and visualized as time, frequency responses, and probability density function (PDF), respectively. Meanwhile, they are transformed into composite images based on the prior research experience of Tang et al. [11]. All images were labeled according to the image features of respective domains. In the input phase, the acceleration data is divided into three groups based on the sensor's measurement direction to facilitate multi-input model requirements. Subsequently, a data classification model utilizing a feature fusion strategy is designed. In the second step, the model employs transfer learning, leveraging pre-trained network parameters, to predict unknown seismic events. Additionally, sensor data from identical time points are grouped, and a global voting decision fusion method is used to determine the precise timing of seismic events accurately.

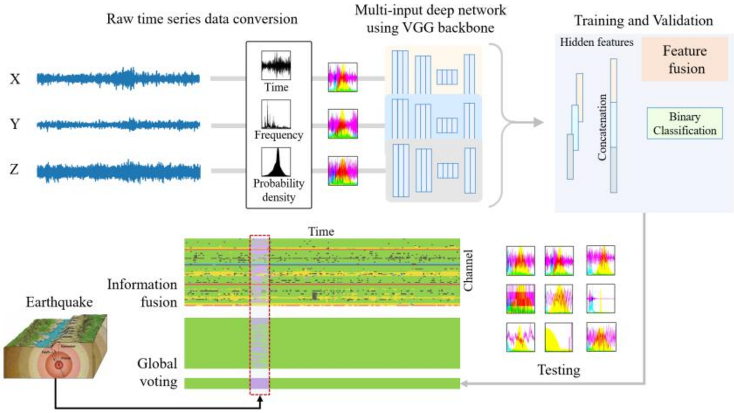

Fig. 1. Workflow of the proposed method

2.1 Time Series Representation in Multiple Image-based Spaces

Monitoring data can be input into neural networks in different representation spaces to enhance the accuracy and efficiency of anomaly detection. In this paper, we follow the vision-based anomaly detection approach to present the monitoring data for neural networks. In terms of model input, sensors are grouped by measurement direction for multi-head input. They are then batched by time to avoid convergence difficulty issues from parallel inputs of many sensors. Fig. 2 illustrates the data structure of the input data. For data space representation, the continuous time series were segmented by a sliding window with an overlap, then plotted in the time, frequency responses, and probability density function, respectively. Three-channel images were created by stacking these images, and the axis labels were removed to enhance the focus on trend analysis over time. Different from other image space-based representation methods, these three spaces are frequently employed in manual inspection due to their high versatility and interpretability. Furthermore, human experts possess adequate background knowledge, and the knowledge acquired by neural networks can align with human experts' daily experiences.

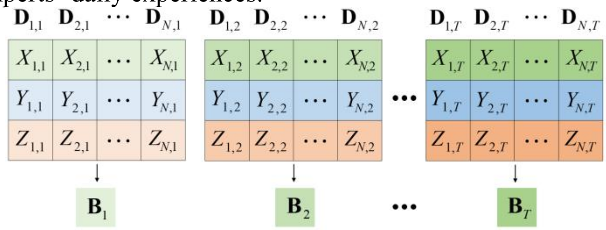

Fig. 2. The data structure of the multi-input CNN model

2.2 Multi-input Convolutional Neural Network

To handle the three-directional monitoring data expressed in time, frequency, and PDF image spaces and output a globally consistent seismic detection result, a multi-input-single-output architecture is constructed using VGG-16 as the backbone [12]. VGG-16 has been extensively utilized and validated across numerous image processing tasks, proving its effectiveness and reliability. Its architecture is simple, easy to understand, and implement, making it suitable for adjustments and optimizations across different application scenarios. Additionally, employing other algorithms is also feasible and can further enhance model performance and adaptability. The paper uses three parallel VGG-16 as input models for three directions, where each direction's sample images are processed on a completely independent VGG-16. Additionally, as a subtask of the multi-input CNN model, each VGG-16 simultaneously outputs the probability of the six patterns of sample images in that direction. The extracted features are then integrated through the feature fusion strategy to improve seismic event detection accuracy further.

The multi-input feature fusion strategy integrates the acceleration data from each measurement direction, providing a more comprehensive representation of seismic events. The limitations of the single sensor system are effectively overcome. The multi-input feature fusion model with three parallel VGG-16 networks as the backbone, integrating all feature vectors into the shared space of the final fully connected layer. These vectors are concatenated to create a new fully connected layer. Assuming the column feature vectors for each direction are v_X , v_Y and v_Z . The concatenated feature vector is obtained by joining and can be represented as

$$v_{fusion} = [v_X, v_Y, v_Z]^T \tag{1}$$

where v_{fusion} is the fused feature vector; v_X , v_Y and v_Z are the original feature vectors of the three directions.

For seismic and non-seismic event identification, the model generates a probability distribution for potential seismic events using a sigmoid function, and a probability score is assigned to the seismic event's occurrence. This score reflects the accuracy of the model's detection capabilities. The error is calculated during training based on the difference between the predicted labels, after feature fusion, and the actual labels. The feature fusion model uses the binary cross-entropy loss to calculate the error at the global fusion stage, which is commonly used in binary classification tasks to measure the difference between two probability distributions.

The total loss consists of the three loss of branches and the loss of feature fusion. This total loss can then be optimized using any backpropagation algorithm.

$$L_{total} = L_X + L_Y + L_Z + L_{fusion} \tag{2}$$

where L_{total} is the total loss of the proposed neural network, L_X , L_Y and L_Z is the loss in each direction, respectively, and L_{fusion} is the loss of feature fusion layer.

3 Example

The acceleration monitoring data from a long-span cable-stayed bridge, consisting of northern and southern branches, were used for method verification. There are a total of 70 channels of acceleration data from the bridge's girders and piers at a sampling frequency of 50 Hz. The locations and directions of the sensors are shown in Fig. 3.

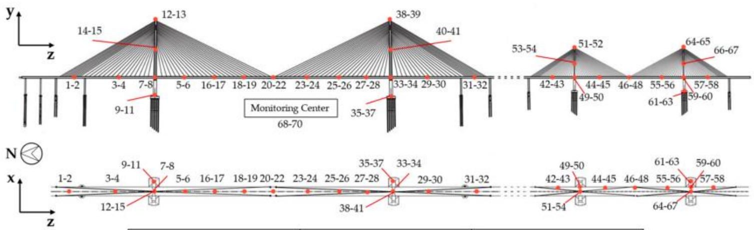

x-direction	y-direction	z-direction
1, 3, 5, 7, 9, 12, 14, 16, 18, 20, 23, 25, 27, 29, 31, 33, 35, 38, 40, 42, 44, 46, 49, 51, 53, 55, 57, 59, 61, 64, 66, 68	2, 4, 6, 11, 17, 19, 22, 24, 26, 28, 30, 32, 37, 43, 45, 48, 56, 58, 63, 70	8, 10, 13, 15, 21, 34, 36, 39, 41, 47, 50, 52, 54, 60, 62, 65, 67, 69

Fig. 3. Sensor locations of the cable-stayed large-span bridge (consists of a northern-branch bridge and a southern-branch bridge)

3.1 Data Collection and Dataset Generation

In this study, we collected acceleration response data from two seismic events for the large-span cable-stayed bridge. A one-hour time series was extracted for each seismic event. This study employed a visual-based anomaly detection method to generate an image dataset. A 30-second sliding window with a 15-second overlap was used to segment the continuous time series. Subsequently, each time segment was visualized in the time domain, frequency domain, and PDF domain to create single-channel images. To serve as input for a 2D CNN, these three types of single-channel images (time domain images, frequency domain images, and PDF images) were superimposed into a single composite image. The dimensions of these time-frequency-PDF images were set to $100 \times 100 \times 3$. It is important to note that the monitoring data contained various anomalies due to system failures. Based on visual features and ground truth conditions, sample images were manually labeled into six patterns: normal, missing, minor, bias, drift, and seismic, with the visual feature descriptions of various data detailed in this paper [13]. Typical samples of the various modes are shown in Fig. 4. Via data conversion, a dataset containing 33,600 labeled samples was built. The specific information for each seismic event is shown in Table 1. Finally, by reusing sensor data in the same direction and creating image sets, a dataset of 15360 labeled sample pairs was constructed. Table 1 shows the number of image sets per pattern for Event 1 and Event 2.

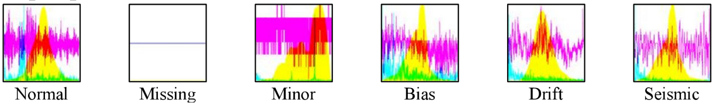

Fig. 4. Examples of normal, seismic, and anomalous patterns

Table 1. Number of each type of samples in each direction and image sets for each event.

Direction	Anomaly Patterns	Event 1	Event2	Total (each event)
X	Normal	2889, 38%	5568, 73%	7680
	Missing	837, 11%	286, 4%	
	Minor	2185, 28%	801, 10%	
	Bias	689, 9%	525, 7%	
	Drift	652, 8%	250, 3%	
	Seismic	428, 6%	250, 3%	
Y	Normal	2482, 52%	3402, 71%	4800
	Missing	703, 15%	406, 8%	
	Minor	926, 19%	509, 11%	
	Bias	454, 9%	428, 9%	
	Drift	102, 2%	3, 0%	
	Seismic	133, 3%	52, 1%	
Z	Normal	1379, 32%	2768, 64%	4320
	Missing	719, 17%	0, 0%	
	Minor	1357, 31%	1151, 27%	
	Bias	305, 7%	232, 5%	
	Drift	348, 8%	24, 1%	
	Seismic	212, 5%	145, 3%	
Image sets	Non-seismic	7416, 96.6%	7483, 97.4%	7680
	Seismic	264, 3.4%	197, 2.6%	

In this study, data labeling does not consider the quantitative values of vibration acceleration but is based on the visual features of sample images. The marking of seismic data primarily relies on two key aspects: Firstly, reference was made to seismic information released by the China Seismic Administration. Due to the propagation characteristics of seismic waves, the bridge's seismic response typically occurs a few seconds after the actual seismic event. Secondly, the seismic response characteristics of large-span bridges exhibit long periods, which is crucial for data processing and analysis. Next, seismic event 1 was used to train the neural network with a training-to-validation ratio of 4:1, and seismic event 2 was used as the test set. Fig. 5 illustrates the distribution of anomalies in acceleration data from three directions during seismic event 1. Additionally, it illustrates the overall temporal distribution of this event, which started around 21:57, followed by an aftershock around 22:12. It is imperative to note that not all vibration acceleration data significantly displayed seismic response characteristics. Some sensor channels were consistently not labeled as showing seismic responses throughout the event. Furthermore, some sensor channels in the three directions failed to record the seismic event due to continuous sensor malfunctions, leading to substantial data loss or only minor responses. Also, the pattern Bias in the data is scattered across the time and space dimensions in all directions, potentially interfering with accurate seismic detection.

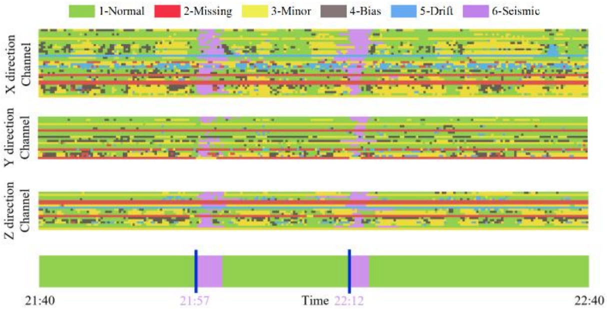

Fig. 5. Visualization of spatial and temporal distribution of sample labels of seismic event No. 1

3.2 Neural Network Training and Validation

In the context of classification tasks, *accuracy* , *precision* , *recall* , and F_1 score are used as key metrics to evaluate the performance of a model. *accuracy* represents the proportion of all correctly predicted samples (positive and negative) out of the total number of samples, serving as the most intuitive measure of overall predictive effectiveness. *precision* , also known as the positive predictive value, refers to the ratio of true positive samples among all samples predicted as positive. This metric focuses on the accuracy of the model in predicting positive classes. *recall* , or true positive rate, measures the proportion of actual positive samples correctly predicted as positive by the model. This metric emphasizes the model's ability to cover positive samples. The F_1 score is a crucial metric for comprehensively assessing the performance of a classification model. It combines precision and recall by taking the harmonic mean of these two metrics, providing a single measure. The F_1 score is particularly suitable for scenarios where precision and recall are equally valued, as it balances these two performance measures. The mathematical expressions for these metrics are as follows:

$$accuracy = \frac{tp+tn}{tp+tn+fp+fn}, \quad precision = \frac{tp}{tp+fp}, \quad recall = \frac{tp}{tp+fn}$$
$$F_1 = \frac{2}{\frac{1}{precision}+\frac{1}{recall}} = 2\frac{precision \cdot recall}{precision + recall} \times 100\% \tag{3}$$

where tp denotes "true positive" (correctly predicted positive classes), fp denotes "false positive" (incorrectly predicted negative classes as positive), tn represents "true negative" (correctly predicted negative classes), and fn represents "false negative" (incorrectly predicted positive classes as negative).

The experiment was conducted on a computer equipped with a 12th Gen Intel(R) Core (TM) i7-12700KF CPU and an NVIDIA RTX3060 GPU. The training was carried out with a batch size of 32 and a learning rate of 0.00001, with 70 epochs performed. A learning rate decay strategy that halves the learning rate every ten iterations was implemented to ensure the stability of the training. Additionally, to prevent model overfitting, an early stopping strategy was employed. The Adam algorithm, which combines the advantages of momentum and adaptive learning rate adjustments, was used to optimize model parameters.

Performance metrics such as accuracy and loss were recorded for the training and validation datasets during each training epoch. The validation accuracy was used as the criterion for selecting the best-performing model. The best performance for the training model was recorded in the 58th epochs, respectively, according to the performance metrics. Specific results are shown in Fig. 6.

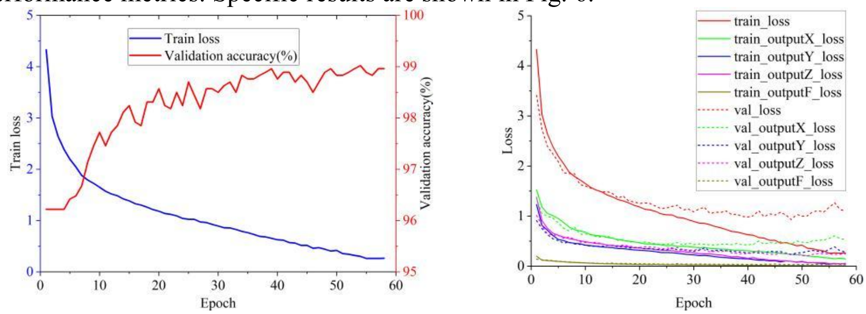

(a) Train loss and validation accuracy (b) Loss

Fig. 6. Loss and validation accuracy

Table 2 shows the model's classification performance on the validation set for acceleration data in different directions under the feature fusion strategy. The feature strategy model achieved effective abnormal data detection, with accuracy exceeding 83% in three directions. For the pattern Seismic, F_1 scores in three directions were above 81%, which suggests a high probability that the monitoring system correctly detects a real seismic event rather than a false alarm due to sensor faults. As shown in Fig. 7(a), the feature fusion strategy generally improved the precision rate and recall rate of the seismic pattern. Meanwhile, the overall accuracy reached 98% by implementing the feature fusion strategy.

3.3 Test using Real-world Seismic Events

To assess the generalization ability of the model, seismic event 2 was utilized for testing, as shown in Table 2. The results show that the accuracy of each direction is above 82%. The highest is in the Y direction, which is 87.9%. For the three directions, the precision rate and recall rate of the pattern Normal and Missing are the highest two patterns. They all reach above 85%. For the seismic pattern, the highest F_1 score in the X direction is 61.3%, respectively. Meanwhile, as shown in Fig. 7(b), the detection of the seismic pattern was significantly improved, with the overall accuracy reaching 98%, by implementing feature fusion strategy. In addition, as shown in Fig. 7(c), the global voting strategy is used to predict seismic events globally. The results show that the model can achieve high seismic detection accuracy throughout the entire time period.

Table 2. Feature fusion model results for validation and test sets in each direction.

Direction	Anomaly Patterns	Accuracy		Precision		Recall		F1 Score	
X	Normal	0.837	0.826	0.880	0.907	0.827	0.877	0.853	0.892
	Missing			0.954	0.857	0.976	0.992	0.965	0.919
	Minor			0.890	0.754	0.867	0.721	0.878	0.737
	Bias			0.405	0.211	0.505	0.243	0.449	0.226
	Drift			0.754	0.864	0.904	0.911	0.822	0.887
	Seismic			0.842	0.476	0.793	0.862	0.817	0.613
Y	Normal	0.935	0.879	0.978	0.961	0.942	0.954	0.960	0.958
	Missing			0.981	0.993	0.986	0.863	0.983	0.923
	Minor			0.945	0.724	0.948	0.612	0.946	0.663
	Bias			0.783	0.384	0.891	0.545	0.834	0.451
	Drift			0.290	0.400	0.529	0.056	0.375	0.098
	Seismic			0.854	0.442	0.789	0.824	0.820	0.575
Z	Normal	0.939	0.843	0.914	0.921	0.938	0.898	0.926	0.909
	Missing			1.000	——	0.996	——	0.998	——
	Minor			0.971	0.827	0.973	0.900	0.972	0.862
	Bias			0.809	0.314	0.742	0.305	0.774	0.310
	Drift			0.914	0.302	0.977	0.098	0.944	0.148
	Seismic			0.913	0.429	0.802	0.858	0.854	0.572

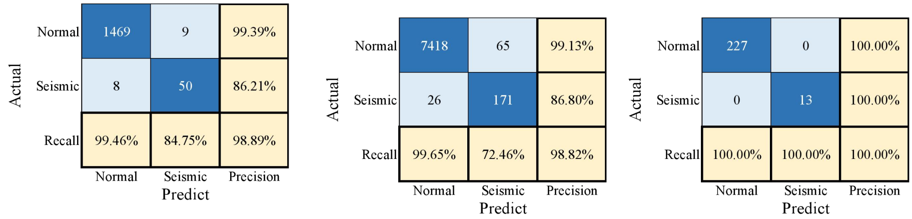

(a) feature fusion (validation set) (b) feature fusion (test set) (c) global voting (test set)

Fig. 7. The confusion matrix of sample pairs on the validation set and test set

4 Discussions

4.1 Panorama of Data Distribution

This section presents and compares the spatiotemporal distribution of the detection results for the second seismic event. As illustrated in Fig. 8, each row displays the data distribution from 70 channels over the total time span, with the sensors grouped according to the measurement directions (X, Y, Z). Additionally, the results of group-based multi-input detection, where each group contains one image from each of the X, Y, and Z directions, are provided. Fig. 8 (a) depicts the distribution of manually labeled data anomalies and seismic events, while Fig. 8 (b) shows the distribution under the feature fusion strategy. It is evident that the detection results align with the actual data anomaly distribution, with the normal data predominating and anomalies being randomly distributed. Similar to the first seismic event, not all sensor channels exhibited seismic response characteristics. The graphs indicate that the feature fusion strategy effectively filtered out seismic samples distributed across time and space, reducing the number of misclassified samples.

Further, a global detection result is obtained by using the voting principle to fuse the detection results of multiple groups at the same moment, as shown in Fig. 8 (c). It shows that the feature strategy model successfully identified the seismic events, showing that the bridge's seismic response began around 13:01, consistent with the groundtruth. The feature fusion detection results for the entire seismic event well matched the actual occurrences. From the distribution of multi-input detection before global voting, it can be seen that these scattered false alarms of individual sensors can be effectively eliminated by global voting.

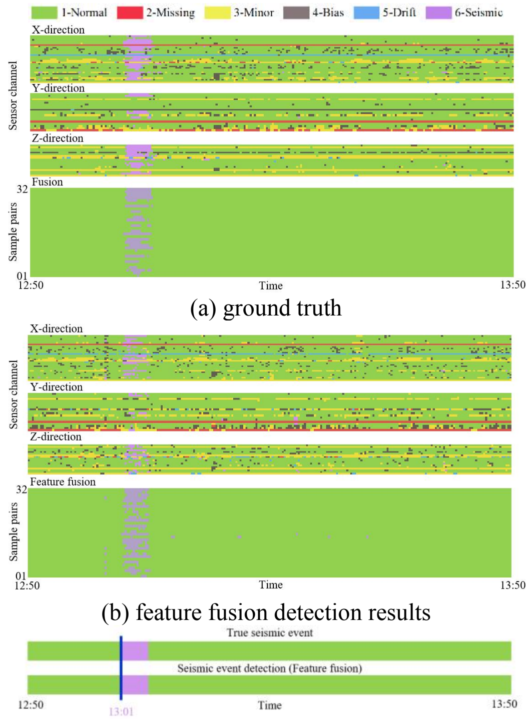

(a) ground truth

(b) feature fusion detection results

(c) comparison of the distribution of No. 2 seismic events.

Fig. 8 Comparison of actual results and detection results in all directions throughout time

4.2 Three-channel Input Ablation Study

This section conducted an ablation experiment to investigate the contribution of each input channel to the overall classification performance. In addition to the original complete three-channel input, i.e., time-frequency-PDF (TFP), one of the three data representation spaces is removed each time to form the other three data inputs: time-frequency (T-F), time-PDF (T-P), frequency-PDF (F-P). Therefore, a total of 4 scenarios were compared in the ablation study.

As shown in Fig. 9, the model with full three-channel inputs is generally better than models trained with any two-channel configuration. In addition, the performance of the two-channel input fusion strategy using frequency and probability density curves is significantly reduced. In addition, the seismic event detection performance with three-channel inputs is better than models trained with any two-channel configuration both before and after global voting.

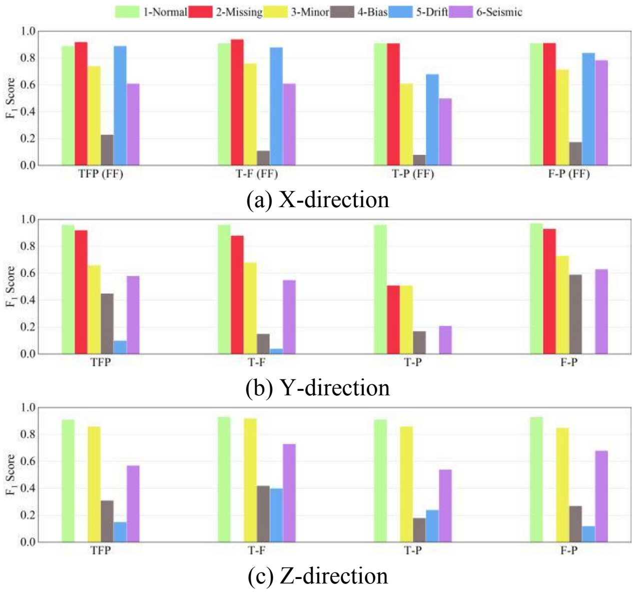

Fig. 9 Comparison of results based on different information sources input to the multi-input model.

5 Conclusion

This paper presents a multi-input deep learning approach for detecting seismic events in large-span bridges. Various types of anomaly interferences in real-world monitoring data are considered. This method presents the raw time series monitoring data into three image space, i.e., time, frequency, and probability density functions (PDF) and then classifies seismic events and anomalies by leveraging graphical features. Moreover, a multi-input CNN was designed to independently receive monitoring data from the X, Y, and Z directions. The feature fusion was developed for the goal accurate seismic event detection.

The feasibility and accuracy of the proposed method were validated using data from two seismic events recorded by the SHM system of a large-span cable-stayed bridge. The dataset includes normal data, seismic data and four types of anomalies: missing, minor, deviation, and drift. Experimental results show that the feature fusion strategy achieved accuracies exceeding 80% in three directions. Through global voting by multiple groups of sensors, the seismic event detection accuracy of feature fusion is further improved to 100%. Furthermore, the study explored the impact of different inputs of data presentation on model performance, and the comparative results confirmed that adding multi-channel inputs can improve the accuracy of data anomaly and seismic event detection.

Acknowledgement

This research was supported by the Yunnan Fundamental Research Projects (Grant No. 202301AT070394, 202301BE070001-037).

References

1. Karakostas, C., Quaranta, G., Chatzi, E.: Seismic assessment of bridges through structural health monitoring: a state-of-the-art review. Bulletin of Earthquake Engineering 22(3), 1309-1357 (2023).
2. Cross, EJ., Koo, Ky., Brownjohn, JMW.: Long-term monitoring and data analysis of the Tamar bridge. Mech Syst Sig Process 35, 16–34 (2013).
3. Khaleghi, B., Khamis, A., Karray, F, O.: Multi sensor data fusion: A review of the state-of-the-art. Information fusion 14(1), 28-44 (2013).
4. Liu, X., Sun, C., Zhou, M.: Reinforcement learning-based multislot double-threshold spectrum sensing with Bayesian fusion for industrial big spectrum data. IEEE Transactions on Industrial Informatics 17(5), 3391-3400 (2020).
5. Zhao, K., Li, L., Chen Z.: A survey: Optimization and applications of evidence fusion algorithm based on Dempster–Shafer theory. Applied Soft Computing 124, 109075(2022).
6. Ribeiro, R, A., Falcao, A., Mora, A.: FIF: A fuzzy information fusion algorithm based on multi-criteria decision making. Knowledge-Based Systems 58, 23-32 (2014).
7. Meng, T., Jing, X., Yan, Z.: A survey on machine learning for data fusion. Information Fusion 57, 115-129 (2020).
8. Liu, X., Wu, Z., Yang, Y.: Information fusion diagnosis and early-warning method for monitoring the long-term service safety of high dams. Journal of Zhejiang University SCIENCE A 139, 687-699 (2012).
9. Chen M, Cai Z and Zeng Y.: Multi-sensor data fusion technology for the early landslide warning system. Journal of Ambient Intelligence and Humanized Computing 148: 11165-11172 (2023).
10. Jeong G, Jung M and Park S.: Contextual multimodal approach for recognizing concurrent activities of equipment in tunnel construction projects. Automation in Construction 158: 105195 (2024).
11. Tang, Z., Chen, Z., Bao, Y.: Convolutional neural network - based data anomaly detection method using multiple information for structural health monitoring. Structural Control and Health Monitoring 26(1), e2296 (2019).
12. Simonyan, K., Zisserman, A.: Very deep convolutional networks for large-scale image recognition. arXiv preprint arXiv:1409, 1556 (2014).
13. Guo, J., Tang, Z., Zhang, C.: An Interpretable Deep Learning Method for Identifying Extreme Events under Faulty Data Interference. Applied Sciences 13(9), 5659 (2023).